PCCP

Accepted Manuscript

ROYAL SOCIETY OF CHEMISTRY

www.rsc.org/pccp

Two-Dimensional Transition-Metal Oxides Monolayers as Cathode Materials for Li and Na Ion Batteries

Chon Chio Leong, Hui Pan*, and Sut Kam Ho

Institute of Applied Physics and Materials Engineering, Faculty of Science and Technology, University of Macau, Macao SAR, P. R. China

Abstract: Two-dimensional monolayers are attractive for applications in metal-ion batteries because of low ion-diffusion barrier and volume expansion. In this work, we carry out first-principles study on electrochemical and structural properties of two-dimensional (2D) oxides monolayers and investigate their applications in metal-ion batteries. 2D transition-metal oxides monolayers (MO_2; M = Mn, Co, and Ni) with various ion-intercalation densities are systematically studied. Our calculations show that Li and Na atoms can easily transport on the surfaces of the monolayers with low diffusion barriers because of long binding distance. We find that Li_2MO_2 and Na_2MO_2 are stable because of negative intercalation energies and unsaturated specific energies. We show that MnO_2 has the lowest diffusion barrier, highest specific capacity, and smallest lattice expansion under Li-intercalation, but lowest cell voltage. We also find that CoO_2 has the largest cell voltages in a wide range of ion-intercalation densities and smallest lattice expansion under Na-intercalation, and NiO_2 only gives the highest cell voltage in Li_2NiO_2 and has largest volume expansion. We further show that Li and Na atoms in Li_2MO_2 and Na_2MO_2 move from stable-adsorption sites to metastable sites on the surfaces of oxides monolayers to reduce lattice expansion, leading to reduced cell voltages. It is

expected that metal-ion batteries with particular applications and performances can be achieved by designing these oxides monolayers.

Keywords: Transition-metal oxide monolayers; Li/Na diffusion; cell voltage and specific capacity; volume expansion; metal-ion battery; first-principles calculation

* H. Pan (huipan@umac.mo); Tel: (853)88224427; Fax: (853)28838314

Introduction

Rechargeable energy storage devices have been in ever-increasing demand as energy sources in huge-amount of portable electronics, commercial electronic vehicles, and large-scale electric networks [1-3]. As a robust technology, metal-ion batteries, especially lithium-ion batteries (LIBs), have been attracting extensive interests because they can deliver high energy, power capacities, and have reasonable stability [4-5]. However, it is a great challenge to develop metal-ion batteries to deal with society's fluctuating energy needs, because of the low abundance of electrode materials. At the same time, the overall performance strongly relies on the structures and properties of the electrode materials. Substantial efforts have been devoted to develop electrode materials with nanostructures, including nanotubes, nanowires, nanoparticles, nanoporous structures, and their composite, because they may enhance energy and power capacities, improve charging/discharging time, and even reduce the cost [6-11]. Recently, two-dimensional (2D) monolayers have attracted increasing attention for their applications into metal-ion batteries as cathodes and anodes due to their particular structural, physical, and chemical properties [12-21]. As anode electrode, layered MoS_2 showed the high-rate transportation of sodium ions due to the short diffusion paths and allows easy Na^+ ion insertion/de-insertion [12]. TiS_3 monolayer showed a lower energy barrier for the diffusion of Na atoms [13]. Much lower energy barriers for metal-ion diffusion could be achieved on 2D transition-metal carbides/nitrides (so called MXenes) [17, 18]. As one of most important components in metal-ion batteries, the cathode plays a determinate role to

their capacities and costs [5]. Currently, layered bulk metal oxides have been widely used in commercial LIBs. The Li/Na ions in layered $LiMO_2$/$NaMO_2$ (M = Ni, Mn, Co, etc.) lie between the sheets of edge-shared MO_6 octahedra [22-34]. However, the preparation of well-ordered structures is difficult and these bulk forms of these layered materials resulted in reduction of capacity. 2D oxide monolayers may provide solutions to solve these issues. The oxides monolayers may have two structures depending on point-group symmetries, including 2H and 1T structures for D_{6h} and D_{3d} point-group symmetries, respectively [35]. Theoretically, Ataca et al. reported that MnO_2 and NiO_2 with 1T structures are stable [36]. Although Ataca et al. reported that CoO_2 monolayer is unstable [36], single-layer CoO_2 could be achieved by Na-intercalation [37]. In this work, we focus on theoretical study of two dimension transition metal oxides MO_2 (M = Mn, Co, and Ni) monolayers as cathode materials for Li and Na batteries based on first-principles calculations. From our calculation results, we show that these monolayers can host high density of Li/Na atoms because of exothermic intercalation and the charging/discharging rate of Na is faster than that of Li. We find that MnO_2 shows fast charging/discharging rate, high specific capacity, and smaller expansion under Li-intercalation, but low cell voltage and larger lattice expansion under Na-intercalation. We further show that CoO_2 has large cell voltage, smaller specific capacity and small volume expansion under Na-intercalation.

Computational Method

The electrochemical properties of 2D transition-metal oxides monolayers are investigated to find their applications as cathode materials in metal-ion batteries based on the density functional theory (DFT) [38] and the Perdew-Burke-Eznerhof generalized gradient approximation (PBE-GGA) [39]. We use the Vienna ab initio simulation package (VASP) [40] incorporated with projector augmented wave (PAW) scheme [41, 42] in the calculations. A 15×15×3 grid for k-point sampling based on the Monkhorst and Pack scheme [43] is used for geometry optimization of unit cells. An energy cut-off of 500 eV is consistently used in our calculations. We employ a vacuum region of 20 Å to isolate the monolayer from its images in neighbouring cells in the vertical direction. Spin-polarized calculations are performed in our calculations. Good convergence is obtained with these parameters and the total energy is converged to 2.0×10^{-5} eV/atom.

Results and Discussion

The 1T 2D transition-metal oxides monolayers (MO_2, M = Mn, Co, and Ni) are constructed as reported in literature [36], where the monolayer is a three-atom-thick layer in a sequence of O-M-O and has D_{3d} point-group symmetry (Figures 1a&b). So, its electrochemical properties are studied for comparison. The monolayers are first fully optimized to obtain their lattice parameters. The relaxed geometries show that the lattice constants of considered 2D oxides monolayers are 2.887, 2.819, and 2.823 Å (Table I). We see that our results on lattice constants are larger than those in

literature [36], because GGA+U was used in their work.

Supercell with 3×3×1 unit cells for oxide monolayer is constructed to find the stable ion-adsorption site (Figure 1). There are three possible positions at one side of the monolayer, including direct top of O atom (TO), top of metal atom (TM), and hexagonal center (HC, opposite top of O atom) (Figure 1). The supercells with one Li/Na ion at all the possible sites are relaxed to find the site of stable adsorption. As an indication of the stable adsorption, the adsorption energy (E_{ad}) is calculated as below:

$$E_{ad} = E(ML + ion) - E(ML) - \mu_{ion} \qquad (1)$$

where *E(ML+ion)* and *E(ML)* are the total energies of the monolayer supercell with and without one Li/Na atom, and μ_{ion} is the energy of Li/Na calculated from the bulk. Our calculations show that the adsorption energies are negative at all of three possible sites on each monolayer supercell, indicating that Li/Na-intercalation is exothermic. We notice that the ion adsorption energy on TO are almost equal to that on TM or HC (Figure 2), except Na on NiO_2 monolayer supercell (Figure 2c). After carefully examining the relaxed structures, we find that Li/Na atom that is initially on the direct top of O atom shifts to other sites, TM or HC, indicating that TO be unstable to host Li/Na atom. Although Na keeps on the top of O atom after relaxation, the adsorption energy (negative) is larger than those on other sites (TM and HC) (Figure 2c), also showing that TO is not favourite to Li/Na atom. We also notice that hexagonal centre (HC) is much stable to hold Li/Na atom because of the strong

adsorption energies (Figure 2). The adsorption energies are -2.54, -3.60 and -2.71 eV for Li on HC of MnO_2, CoO_2, and NiO_2, respectively, and -2.38, -3.40 and -2.56 eV for Na on HC of MnO_2, CoO_2, and NiO_2, respectively (Figure 2). We see that the Li/Na adsorption on CoO_2 monolayer is stronger than those on other oxides monolayers. From the relaxed systems, we find that the Li-O distances are 1.98, 1.95 and 1.97Å for Li on MnO_2. CoO_2, and NiO_2, respectively, and the Na-O distances are 2.33, 2.30 and 2.31Å on MnO_2. CoO_2, and NiO_2, respectively. We see that the Li-O distance in Li-adsorbed MnO_2 supercell is the longest in all three oxides systems and may suggest easy Li diffusion and fast charging/discharging on MnO_2 (Table II). The Na-O distance is larger than Li-O distance on each system, indicating that Na-diffusion is easier than Li-diffusion.

The longer binding distances indicate that these 2D metal oxide monolayers are suitable for metal-ion batteries. Ion diffusion is one of key issues for their applications in batteries, which is responsible to the charging/discharging process. Therefore, it is necessary to calculate ion-diffusion barriers on these monolayers. In our calculations, the ion-diffusion barrier is calculated by moving one Li/Na atom from one stable adsorption site to another via a metastable adsorption site, which shows the lowest energy barrier [13, 15, 44]. Because the most stable and metastable adsorption sites on each monolayer are the hexagonal center (HC) and top of metal atom (TM), respectively, the easiest paths should be HC – TM – HC (red dots 0 – 3 – 6 in Figure

3). As Li atom moving from the most stable adsorption site (0) to metastable site (3), we see that energy barriers increasingly reach to the maximums at 2/3 on the path from 0 to 3 (as indicated in Figure 3) and then decrease (Figure 4a). We find that the Li-diffusion barrier on CoO_2 and NiO_2 supercells are almost equal to each other. The Li-diffusion barrier on MnO_2 monolayer is the lowest (0.16 eV) (Figure 4a), resulting in fast Li-charging/discharging process in MnO_2. The Na-diffusion barriers on three oxide monolayers are ~ 0.12 eV with a difference of 0.008 eV from each other (Figure 4b), which are lower than Li-diffusion barrier, indicating the charging/discharging of Na ions is faster than that of Li ions. From the calculated binding distance and adsorption energy (Table II) and diffusion energies (Figure 4a and 4b), we see that the diffusion energy decreased as the binding energy decreases and binding distance increases. When the binding energy is small and binding distance is larger, the Li/Na ions can pass through the materials fast, and easy, resulting in low diffusion barrier. Therefore, by considering diffusion barrier, binding distance, and adsorption energy, we see that Lithium/Sodium atoms are easy to transport on MnO_2 monolayer, resulting in fast charging/discharging during Li/Na-intercalation/decalation processes. We found that our calculated Li-diffusion barrier on MnO_2 monolayer (0.156 eV) is consistent with a recent publication (0.148 eV) [45].

To investigate the Li/Na-ion storage capacities in these 2D oxides monolayers, we study their electrochemical properties under various intercalation densities. A number

of electrochemical properties can be derived directly from the difference in total energies before and after lithium intercalation – a procedure offering improved accuracy through the cancellation of errors. The intercalation energy (E_{int}), as an indication for the stable storage of Li, is calculated from

$$E_{\text{int}} = (E_{tot}(ML + nIon) - E_{tot}(ML) - n\mu_{Ion})/n \qquad (2)$$

where $E_{tot}(ML+nIon)$ and $E_{tot}(ML)$ are the total energies of the monolayers with and without Li/Na atoms, respectively. n is the number of Li/Na atoms or the Li/Na density. When n = 1 in equation (2), the intercalation energy is the same as the adsorption energy (equation (1)). The change of ion-intercalation density is realized by increasing the number of Li/Na atoms in the supercells or reducing the sizes of monolayer cells. Cells with 3×3×1 units, 2×2×1 units, and 1×1×1 unit are used to study low, medium, and high ion-intercalation densities, respectively. The 3×3×1 and 2×2×1 supercells were constructed based on the lattice parameter of oxide unit cell and kept fixed under Li-intercalation at low and medium densities. The 1×1×1 cells with high Li density were fully relaxed to investigate volume expansion. For convenience, the Li and Na intercalated oxides monolayers are named as Li_xMO_2 and Na_xMO_2, respectively, where $x = \frac{n}{the\ number\ of\ units\ in\ the\ cell}$. Our calculations show that the Li-intercalation energy on each 2D oxide monolayer is negative, which increases as the increment of Li-density initially and converges to a constant (Figure 5a). The negative energy ($E_{int} < 0$) corresponds to exothermic chemical intercalation, leading to stable dissociation of Li bulk and separation of Li atoms. The

Li-intercalation energy on 2D CoO_2 monolayer is lower than that on NiO_2 within a Li-density (x) from 0 to 1 (Figure 5a). At the highest Li-density, the E_{int} on CoO_2 is larger than that on NiO_2 by 0.27 eV and less than that on MnO_2 by 0.74 eV. The E_{int} on MnO_2 is higher than that on NiO_2 in the whole range of considered Li-density (x = 0~2). Therefore, Li atoms are easy to be dissociated and stably separated on CoO_2 monolayer under low and medium Li-densities. The calculated formation energy of the Li bulk is around -1.9 eV and the Li-adsorption energy on CoO_2 is -3.6 to 2.0 eV as x changes from 0.11 to 1. We can see the adsorption of Li on CoO_2 is much stronger than that to form bulk. Therefore, Li atoms can easily be dissociated on CoO_2. We also find that the intercalation energy of Li_2NiO_2 is lower than that of $LiNiO_2$ (Figure 5). We see that the lattice parameters are expanded under ion-intercalation at high Li-density. The lattice constant (a) of the Li_2NiO_2 (3.072 Å) is larger than that of $LiNiO_2$ (2.969 Å) and the lattice constant (a) of Li_xMnO_2 expands from 2.176 to 2.322 Å as x changes from 1 to 2 when Li atoms at HC positions, and the thicknesses also increase (Tables III & IV), leading to the lower intercalation energy. We see that the intercalation energy strongly depends on the lattice parameters, but the variation at high ion-density is smaller. Similar to Li-intercalation, the Na-intercalations on 2D oxides monolayers are also exothermic in the whole considered range of Na-density because of negative intercalation energies, resulting in stable dissociation of Na bulk and separation of Na atoms (Figure 5b). Similarly, the Na-intercalation energy on each oxide monolayer increases initially and reaches to a constant as Na-density (x) increases from 0 to 2 (Figure 5b). We see that the Na-intercalation energy on CoO_2

monolayer is lower than that on NiO_2, and the Na-intercalation energy on NiO_2 monolayer is lower than that on MnO_2. At highest Na-density (x = 2), the E_{int} on CoO_2 is less than that on NiO_2 by 0.15 eV, and that on MnO_2 by 0.25 eV. Same as the Li-intercalation, the intercalation energy of Na_2MnO_2 is lower than that of $NaMnO_2$, which is contributed to the expanded lattice parameters of Na_xMnO_2 (Tables III and IV). If considering intercalation energies only, CoO_2 monolayer is the best candidate as electrode materials in metal-ion batteries. To confirm the stability of ion-intercalated oxides monolayers, the specific energies (E_s) are calculated as below:

$$E_s = -(E_{tot}(ML + nIon) - E_{tot}(ML))/m \qquad (3)$$

where m is the total number of transitional metal and oxygen atoms in the cell. We find that the specific energy increases with the intercalation density (x) (Figure 6). As the intercalation energy is negative in the whole range of the considered intercalation density, we confirm that the Li/Na density may be as high as 2 on a single monolayer. We find that the lattice expansion under high Na-interaction is stronger than that under Li-interaction (Table IV), which may result in the lower specific energies of Na_xMO_2 at x=1.

For practical applications in metal-ion batteries, cell voltage and specific capacity need to be evaluated. The cell voltage (V) and specific capacity (J) are calculated from $V = |\frac{E(Ion_xMO_2) - E(MO_2) - x\mu_{Ion}}{x}|$, and $J = \frac{Q \times F}{3.6 * M}$, where $E(Ion_xMO_2)$ and $E(MO_2)$ are

218 the total energies of 2D oxide monolayer with and without Li/Na-intercalation, Q is
219 the number charge released, *F* is Faraday constant, and *M* is the atomic mass (g/mol).
220 The cell voltage is actually equal to the absolute value of intercalations energy
221 (equation (2)). We see that the cell voltage decreases as the increment of
222 ion-intercalation density (Figure 7). At the highest density, the Li-cell voltages are
223 about 1.18, 1.92 and 2.20 V for MnO_2, CoO_2, and NiO_2, respectively (Figure 7a) and
224 the Na-cell voltages are 0.54, 0.78 and 0.63 V (Figure 7b and Table V). We see that
225 the cell voltages of Li_2NiO_2 and Na_2MnO_2 are higher than those of $LiNiO_2$ and
226 $NaMnO_2$ due to larger lattice expansion. The specific capacity of MnO_2 (617 $mAhg^{-1}$)
227 is the highest at the same Li/Na density because of smaller atomic mass (Table I). If
228 considering voltage cell, CoO_2 monolayer is better than MnO_2 and NiO_2 as cathode
229 for Li-ion and Na-ion batteries because its voltage is higher than others in a wide
230 range of ion density (Figure 7). However, MnO_2 monolayer is the best choice when
231 considering specific capacity.

232

233 Beside the electrochemical properties, the volume expansion during ion-intercalation
234 is also a very important issue to practical application. At high ion-intercalation density,
235 the ion-ion interaction may result in ion-migration on these monolayers. To check out
236 the stable adsorption, two possible adsorption sites, HC and TM, are considered in
237 these unit cells (Li_2MO_2 and Na_2MO_2), which are fully optimized to obtain lattice
238 parameters and find the stable adsorption states. Our calculations show that the

energies of unit cells with ions on HC positions are lower than those on TM sites (Table III), indicating that ions (Li and Na) still prefer on HC sites. We find that the lattice constants of the unit cells with Li atoms at HC positions are expanded by 0.35 % in Li_2MnO_2, 7.34 % in Li_2CoO_2, and 8.82 % in Li_2NiO_2, respectively (Table III). At the same time, the thicknesses (O-O distance in vertical direction) are expanded by 22.2 % in Li_2MnO_2, 36.6 % in Li_2CoO_2, and 28.9 % in Li_2NiO_2, respectively (Table III). Interestingly, we find that the lattice constant of MnO_2 with Li atoms at TM positions shrinks by 2.91 %, and the expansions of the lattice constants of CoO_2 (2.20 %) and NiO_2 (3.86 %) with Li atoms at TM positions are smaller than those at HC positions, but the expansions of their thicknesses (25.2 % in MnO_2, 41.0 % in CoO_2, and 39.2 % in NiO_2,) are increased (Table III). We see that Li-intercalation leads to very small lateral expansion in MnO_2 with Li atoms at HC positions, but large shrinkage if Li atoms take TM positions. Considering both the adsorption energy and lattice change, we predict that Li atoms will occupy HC positions on MnO_2 monolayer during Li-intercalation. Comparing the lattice constants of CoO_2 and NiO_2 with different Li-adsorption positions, we see that their expansions with Li atoms at TM are much smaller than those at HC positions. Although the stable Li-adsorption sites on CoO_2 and NiO_2 monolayers are at HC, Li atoms may immigrate to TM positions to avoid larger lattice expansions. It is, therefore, Li atoms will occupy TM positions on CoO_2 and NiO_2 monolayers at high intercalation-density. Accordingly, the estimated cell voltages of CoO_2 and NiO_2 monolayers with highest intercalation-density reduce to 1.56 and 1.73 V, respectively (Table V).

Similarly, Na atoms still prefer to HC positions on these oxides monolayers (Table III). For Na atoms at HC positions, the lattice constants of MnO_2, CoO_2, and NiO_2 are expanded by 11.4, 7.1, and 13.0 %, respectively (Table III), and their thicknesses are expanded by (16.6 % in MnO_2, 2.5 % in CoO_2, and 10.4 % in NiO_2). For Na atoms at TM positions, the lattice constants of MnO_2, CoO_2, and NiO_2 are expanded by 7.5, 5.1, and 7.9 %, respectively (Table II), and their thicknesses are expanded by (15.9 % in MnO_2, 5.0 % in CoO_2, and 14.0 % in NiO_2). Different from Li-intercalation, we see that Na-intercalation results in less volume expansion of CoO_2 monolayer than other oxides. Although Na atoms prefer to HC sites on these monolayers, they may migrate to TM sites to reduce larger lattice expansions at high intercalation-density. The calculated Na-intercalation energies (E_{int} = - V) of these oxides monolayers with Na atoms at TM sites are higher than those at HC sites, leading to lower cell voltages (Table V).

Based on our calculations and analysis on the electrochemical and structural properties of the 2D oxides monolayers under metal-ion intercalations, we see that each 2D oxide monolayer has its own advantages for application in batteries. For example, MnO_2 monolayer shows fastest ion-diffusion, highest specific capacity, and smallest expansion in Li-intercalation. CoO_2 monolayer gives highest Li-cell and Na-cell voltages in a wide range of metal-ion density, and smallest lattice expansion

under high Na-intercalation density. Our results are consistent with experimental results on layered oxides [34], where CoO_2 has a high cell potential and MnO_2 is more stable than CoO_2 and NiO_2. According to specific requirements, we can choose the particular oxide monolayer as electrode materials in metal-ion batteries.

Conclusion

DFT-based first-principles calculations are carried out to investigate the electrochemical and structural properties of 2D transition-metal oxides monolayers and their application Li-ion and Na-ion batteries. We find that metal ions (Li and Na) prefer to occupy the hexagonal centers on 2D oxides monolayers. The diffusion barriers can be as low as 0.15 eV for Li and ~0.12 eV for Na on MnO_2 monolayer, indicating fast charging/discharging processes. We show that Li_2MO_2 and Na_2MO_2 are stable, leading to high ion-storage capacities. Our calculations also show that CoO_2 has the highest cell voltage in a wide range of metal-ion density and MnO_2 has the highest specific density. We also find that metal ions may migrate from stable adsorption sites to metastable sites to reduce lattice expansion, leading to reduced cell voltage. We further show that MnO_2 has less volume expansion (< 0.35 %) under high Li-intercalation density, indicating stability in the Lithium-ion-intercalation/decalation processes. Our results predict that oxide monolayer can be designed to satisfy the particular requirements for practical applications in metal-ion batteries.

302 Acknowledgments

303 Hui Pan thanks the support of the Science and Technology Development Fund from
304 Macau SAR (FDCT-068/2014/A2, FDCT-132/2014/A3, and FDCT-110/2014/SB) and
305 Multi-Year Research Grant (MYRG2014-00159-FST and MYRG2015-00017-FST)
306 from Research & Development Office at University of Macau. The DFT calculations
307 were performed at High Performance Computing Cluster (HPCC) of Information and
308 Communication Technology Office (ICTO) at University of Macau.

309

310 Sut Kam Ho thanks support from the Science and Technology Development Fund of
311 Macao SAR under grant number 045/2014/A1 and Multi-year Research Grant,
312 University Research Committee, University of Macau under grant number
313 MYRG2015-00042-FST.

References

[1] Q. Tang and Z. Zhou, *Prog. Mater. Sci.*, 2013, **58**, 1244–1315.

[2] P. Roy and S. K. Srivastava, *J. Mater. Chem. A*, 2015, **3**, 2454–2484.

[3] X. Li and C. Wang, *J. Mater. Chem. A*, 2013, **1**, 165–182.

[4] M. D. Bhatt and C. O'Dwyer, *Phys. Chem. Chem. Phys.*, 2015, **17**, 4799–4844.

[5] http://www.epa.gov/oms/climate/documents/bat-pa-c-v2- beta.xlsx

[6] H. Pan, *J. Phys. Chem. C*, 2014, **118**, 9318–9323.

[7] H. Hu, L. Yu, X. Gao, Z. Lin and X. W. (David) Lou, *Energy Environ. Sci.*, 2015, **8**, 1480–1483.

[8] T. Lan, J. Dou, F. Xie, P. Xiong and M. Wei, *J. Mater. Chem. A*, 2015, **3**, 10038–10044.

[9] A. O. Pereira and C. R. Miranda, *J. Phys. Chem. C*, 2015, **119**, 4302–4311.

[10] L. Zhang, H. B. Wu and X. W. D. Lou, *Adv. Energy Mater.*, 2013, **4**, 1300958.

[11] Z. Sun, F. Lv, L. Cao, L. Liu, Y. Zhang and Z. Lu, *Angew. Chem.*, 2015, **127**, 8055–8059.

[12] D. Su, S. Dou and G. Wang, *Adv. Energy Mater.*, 2014, **5**, 1401205.

[13] J. Wu, D. Wang, H. Liu, W.-M. Lau and L.-M. Liu, *RSC Adv.*, 2015, **5**, 21455–21463.

[14] X.-Y. Yu, H. Hu, Y. Wang, H. Chen and X. W. D. Lou, *Angew. Chem.*, 2015, **127**, 7503–7506.

[15] Z.-K. Tang, Y.-N. Zhang, D.-Y. Zhang, W.-M. Lau and L.-M. Liu, *Scientific Reports*, 2014, **4**, 7007.

[16] Y. Liu, M. Zhu and D. Chen, *J. Mater. Chem. A*, 2015, **3**, 11857–11862.

[17] H. Pan, *J. Mater. Chem. A*, 2015, **3**, 21486–21493.

[18] Q. Tang, Z. Zhou and P. Shen, *J. American Chem. Soc.*, 2012, **134**, 16909–16916.

[19] Y. Jing, Z. Zhou, C. R. Cabrera and Z. Chen, *J. Mater. Chem. A*, 2014, **2**, 12104.

[20] Y. Xie, M. Naguib, V. N. Mochalin, M. W. Barsoum, Y. Gogotsi, X. Yu, K.-W. Nam, X.-Q. Yang, A. I. Kolesnikov and P. R. C. Kent, *J. American Chem. Soc*, 2014, **136**, 6385–6394.

[21] J. Su, Y. Pei, Z. Yang and X. Wang, *RSC Adv.*, 2014, **4**, 43183–43188.

[22] A. Kraytsberg and Y. Ein-Eli, *Adv. Energy Mater.*, 2012, **2**, 922–939.

[23] D. Kim, J. R. Croy and M. M. Thackeray, *Electrochem. Commun.*, 2013, **36**, 103–106.

[24] W. K. Pang, S. Kalluri, V. K. Peterson, S. X. Dou and Z. Guo, *Phys. Chem. Chem. Phys.*, 2014, **16**, 25377–25385.

[25] D. A. Tompsett and M. S. Islam, *Chem. Mater.*, 2013, **25**, 2515–2526.

[26] C. Cao, L. Xi, K. L. Leung, M. Wang, Y. Liu, R. Ma, S. Yang, Z. Lu and C. Y. Chung, *RSC Adv.*, 2015, **5**, 30507–30513.

[27] L. Xi, C. Cao, R. Ma, Y. Wang, S. Yang, J. Deng, M. Gao, F. Lian, Z. Lu and C. Y. Chung, *Phys. Chem. Chem. Phys.*, 2013, **15**, 16579.

[28] K. Iwaya, T. Ogawa, T. Minato, K. Miyoshi, J. Takeuchi, A. Kuwabara, H. Moriwake, Y. Kim and T. Hitosugi, *Phys. Rev. Lett.*, 2013, **111**.

[29] M. S. Islam and C. A. J. Fisher, *Chem. Soc. Rev.*, 2014, **43**, 185–204.

[30] A. M. Abakumov, A. A. Tsirlin, I. Bakaimi, G. Van Tendeloo and A. Lappas, *Chem. Mater.*, 2014, **26**, 3306–3315.

[31] M. Shirpour, J. Cabana and M. Doeff, *Energy Environ. Sci.*, 2013, **6**, 2538.

[32] K. Mukai, Y. Kishida, H. Nozaki and K. Dohmae, *Chem. Mater.*, 2013, **25**, 2828–2837.

[33] H. Ben Yahia, M. Shikano and H. Kobayashi, *Chem. Mater.*, 2013, **25**, 3687–3701.

[34] M. S. Whittingham, *Chem. Rev.* 2004, **104**, 4271-4301.

[35] N. V. Podberezskaya, S. A. Magaril, N. V. Pervukhina and S. V. Borisov, *J. Struc. Chem.*, 2011, **42**, 654–681.

[36] C. Ataca, H. Şahin and S. Ciraci, *J. Phys. Chem. C*, 2012, **116**, 8983–8999.

368 [37] K. Takada, H. Sakurai, E. Takayama-Muromachi, F. Izumi, R. A. Dilanian and T.
369 Sasaki, *Nature*, 2003, **422**, 53-55.

370 [38] P. Hohenberg and W. Kohn, *Phys. Rev.*, 1964, **136**, B864–B871.

371 [39] P. E. Blöchl, *Phys. Rev. B*, 1994, **50**, 17953–17979.

372 [40] G. Kresse and J. Furthmüller, *Phys. Rev. B*, 1996, **54**, 11169–11186.

373 [41] J. P. Perdew, K. Burke and M. Ernzerhof, *Phys. Rev. Lett.*, 1996, **77**, 3865–3868.

374 [42] G. Kresse and D. Joubert, *Phys. Rev. B*, 1999, **59**, 1758–1775.

375 [43] W. Lin, H. Spalt and B. W. Batterman, *Phys. Rev. B*, 1976, **13**, 5158–5169.

376 [44] D. Wang, L. M. Liu, S. J. Zhao, B. H. Li, H. Liu and X. F. Lang, *Phys. Chem.*
377 *Chem. Phys.*, 2013, 15, 9075-9083

378 [45] S. Deng, L. Wang, Y. Li, *J. Phys Chems C*, 2015, **119**, 28783-28788

379 [46] G. Ramos-Sanchez, A. Callejas-Tovar, L.G. Scanlon and P. B. Balbuena, *Phys.*
380 *Chem. Chem. Phys.*, 2014, **16**, 743

381

Table I. Calcualted lattice constant of the unit cells of CoO_2, MnO_2 and NiO_2 and their thicknesses (O-O distance in vertial direction, D), M-O bond length (D_{M-O}), and specific capacity at highest ino-inercalation density.

	a (Å)	D (Å)	D_{M-O} (Å)	Specific Capacity ($mAhg^{-1}$)
MnO_2	2.887	1.900	1.920	617
CoO_2	2.819	1.898	1.876	560
NiO_2	2.823	1.867	1.883	591

Table II. Calculated adsorption energy, Li-O and Na-O distances, and diffusion barrier in these oxides 3×3×1 supercells.

	E_{ad_Li} (eV)	Li – O distance (Å)	Li diffusion barrier (eV)	E_{ad_Na} (eV)	Na – O distance (Å)	Na diffusion barrier (eV)
MnO_2	-2.54	1.978	0.156	-2.38	2.325	0.121
CoO_2	-3.60	1.949	0.180	-3.40	2.295	0.122
NiO_2	-2.71	1.969	0.186	-2.56	2.310	0.129

Table III. Calculated lattice constant (a), layer thickness (O-O distance in vertical direction, D), and M-O (D_{M-O}), Li-O (D_{Li-O}) and Na-O (D_{Na-O}) distances in systems with highest ion-intercalation density, and the energy difference of systems with Li/Na at two different adsorption sites (HC and TM). HC: hexagonal center; TM: Top of metal.

	a (Å)		D (Å)		D_{M-O} (Å)		D_{Li-O} *or* D_{Na-O} (Å)		E_{HC}-E_{TM} *(eV/unit)*
	HC	TM	HC	TM	HC	TM	HC	TM	
Li_2MnO_2	2.897	2.803	2.322	2.378	2.037	2.011	1.920	1.980	-0.327
Na_2MnO_2	3.215	3.102	2.215	2.202	2.160	2.100	2.280	2.426	-0.284
Li_2CoO_2	3.026	2.881	2.593	2.676	2.163	2.136	1.853	1.887	-0.721
Na_2CoO_2	3.019	2.964	1.946	1.993	1.996	1.981	2.305	2.389	-0.288
Li_2NiO_2	3.072	2.932	2.407	2.599	2.142	2.132	1.870	1.898	-0.943
Na_2NiO_2	3.191	3.045	2.062	2.129	2.112	2.055	2.214	2.382	-0.471

392

393 Table IV. The lattice constant (a), layer thickness (O-O distance in vertical direction,
394 D), M-O distance (D_{M-O}) and intercalation energy of oxide monolayer unit cells with
395 one Li/Na at HC adsorption sites.

	a (Å)	*D (Å)*	D_{M-O} *(Å)*	E_{int} *(eV)*
$LiMnO_2$	2.880	2.176	1.898	-1.114
$NaMnO_2$	2.935	1.998	1.921	-0.327
$LiCoO_2$	2.886	2.123	2.069	-2.039
$NaCoO_2$	2.924	1.900	1.894	-0.940
$LiNiO_2$	2.969	2.109	1.909	-1.899
$NaNiO_2$	2.983	1.933	1.927	-0.721

396 Table V. Calculated cell voltages (V) of these oxides monolayers with metal ions at
397 different adsorption sites (HC and TM) in unit cells.

	Cell Voltage (V)	
	HC	TM
$LiMnO_2$	1.114	0.911
Li_2MnO_2	0.978	0.814
$NaMnO_2$	0.327	0.226
Na_2MnO_2	0.479	0.337
$LiCoO_2$	2.039	1.817
Li_2CoO_2	1.923	1.563
$NaCoO_2$	0.940	0.818
Na_2CoO_2	0.880	0.736
$LiNiO_2$	1.899	1.552
Li_2NiO_2	2.199	1.728
$NaNiO_2$	0.721	0.488
Na_2NiO_2	1.020	0.784

398

399 Figure caption:

400 Figure 1,Schematic structure of MO_2 (M= Co, Mn, and Ni): (a) top and (b) side views.
401 The yellow circles indicate possible adsorption sites for Li and Na in supercell.

402 Figure 2, Calculated adsorption energies for metal ions (Li and Na) at different
403 positions on the monolayers: (a) MnO_2, (b) CoO_2, and (c) NiO_2.

404 Figure 3, The metal ion diffusion path between two stable adsorption sites via a
405 metastable site. The yellow circles and numbers show intermediate steps.

406 Figure 4, Calculated (a) Li and (b) Na diffusion barriers on the surfaces of: MnO_2,
407 CoO_2, and NiO_2.

408 Figure 5, Calculated intercalation energies for (a) Li_xMO_2 and (b) Na_xMO_2 (M= Co,
409 Mn, and Ni) as a function of ion density (x).

410 Figure 6, Calculated specific energies for (a) Li_xMO_2 and (b) Na_xMO_2 (M= Co, Mn,
411 and Ni) as a function of ion density (x).

412 Figure 7, Calculated cell voltage for (a) Li_xMO_2 and b) Na_xMO_2 (M= Co, Mn, and Ni)
413 as a function of ion density (x).

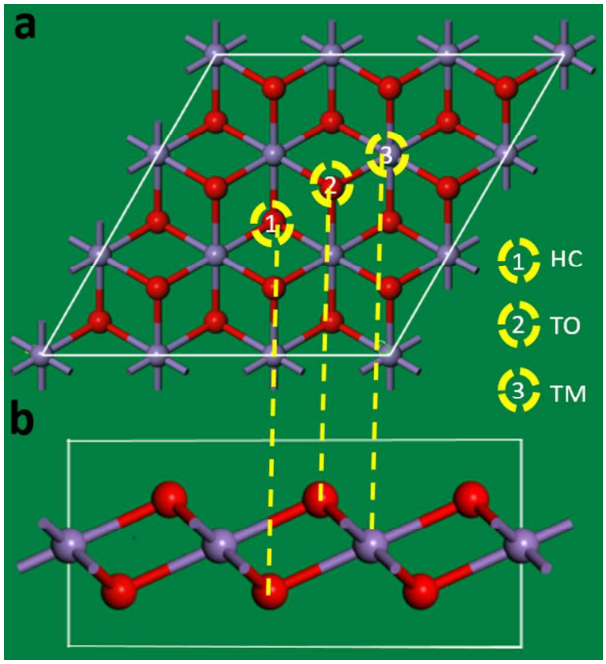

Figure 1

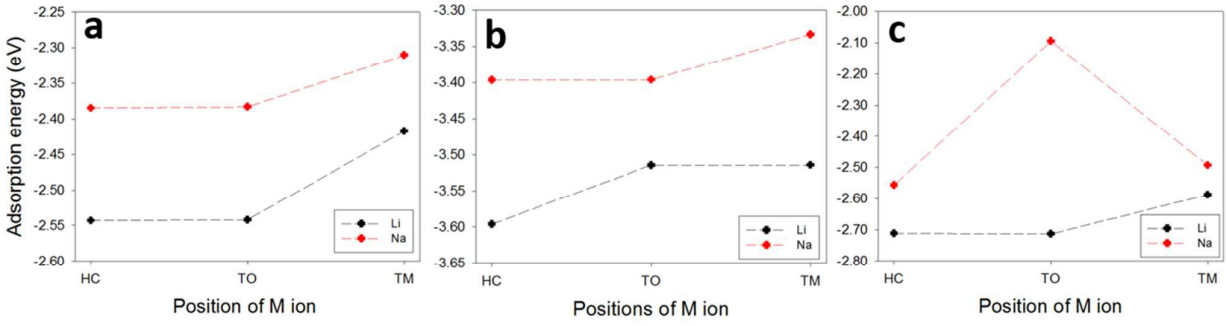

Figure 2

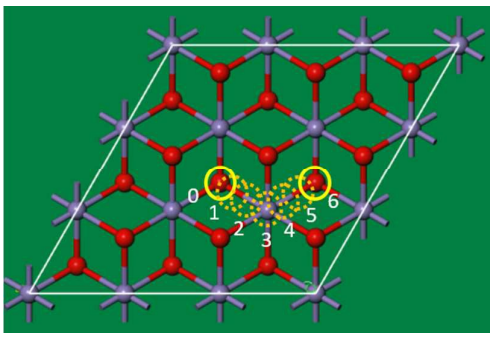

Figure 3

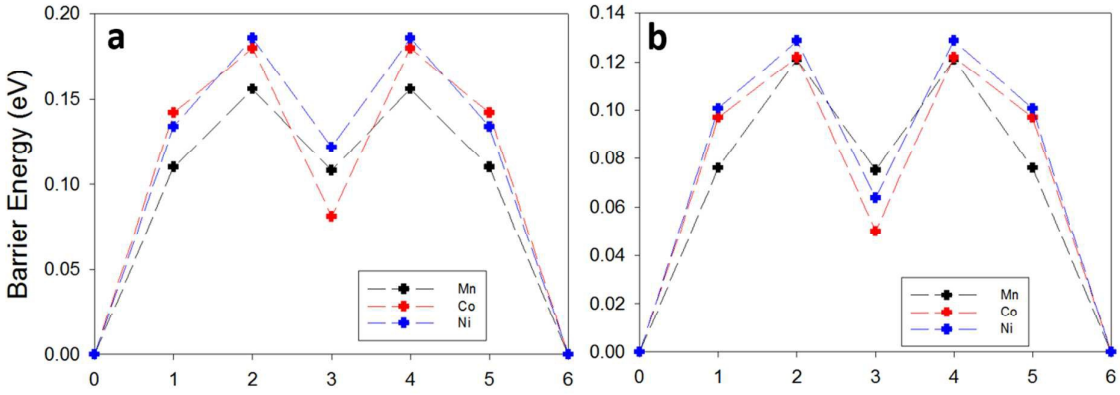

Figure 4

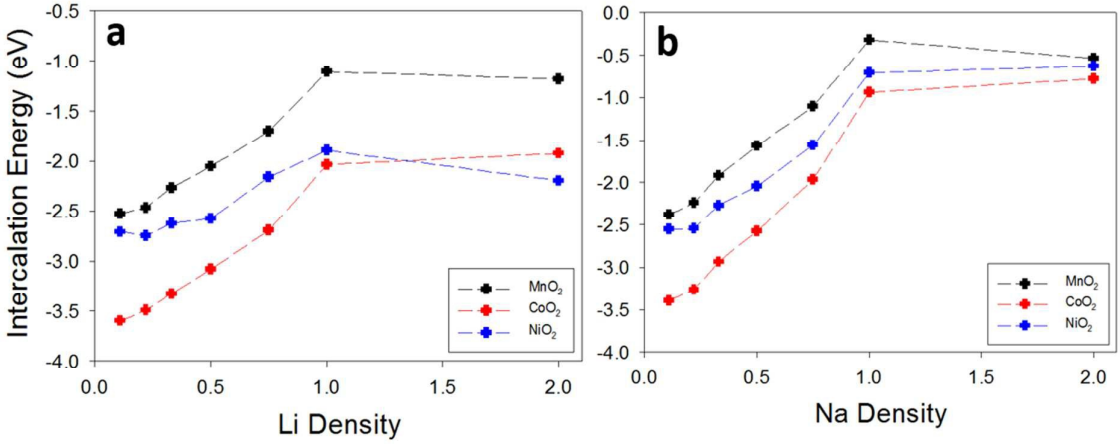

Figure 5

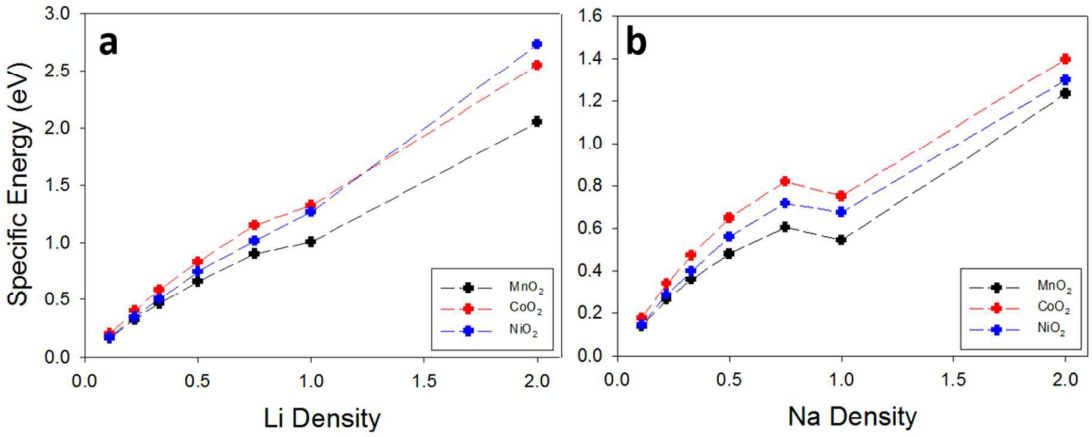

Figure 6

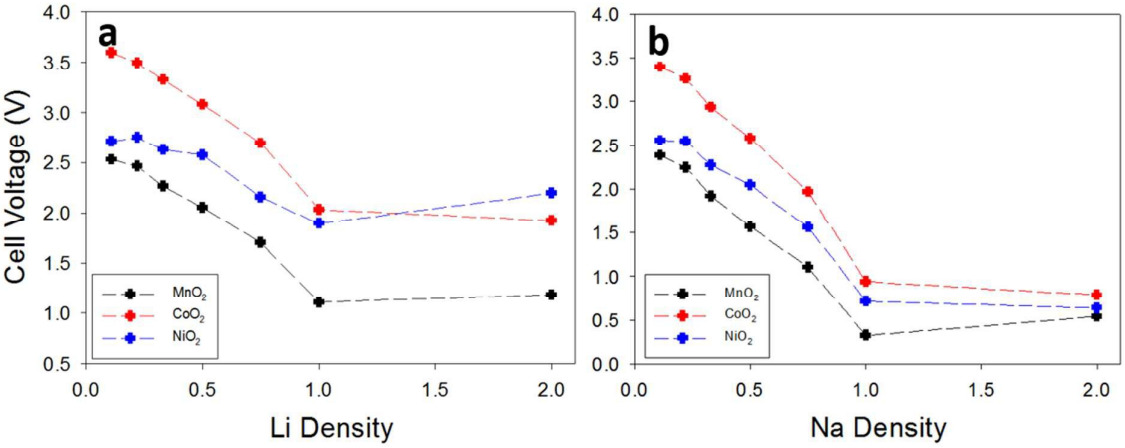

Figure 7